ADVANCED OPTICAL MATERIALS
www.advopticalmat.de

Resonance Effect in Brunel Harmonic Generation in Thin Film Organic Semiconductors

*Weiwei Li, Ahmad Saleh, Manas Sharma, Christian Hünecke, Marek Sierka, Marcel Neuhaus, Lina Hedewig, Boris Bergues, Meshaal Alharbi, Hadi ALQahtani, Abdallah M. Azzeer, Stefanie Gräfe, Matthias F. Kling, Abdullah F. Alharbi, and Zilong Wang**

Nonlinear optical properties of organic semiconductors (OSCs) have been extensively investigated in the perturbative regime, while strong light induced high-order processes in solid-state OSCs are less studied. Here, below-threshold harmonic generation is examined, both experimentally and theoretically, in two solid-state thin film OSCs, that is, tetraphenylporphyrin and zinc tetraphenylporphyrin. Results show that the π–π^* excitations of the porphyrin ring system generate the harmonic emission. The contribution of the Brunel harmonic to the 5th harmonic emission is uncovered, where the resonant 5-photon transition ($S_0 \rightarrow S_2$ transition) is found to lead to an early onset of non-perturbative behavior. A similar resonance effect is expected in Brunel harmonic generation in other organic materials.

1. Introduction

Strong-field nonlinear optical processes have been subject of extensive investigations in a variety of material systems. For instance, high harmonic generation (HHG) in gas-phase atoms and molecules is widely studied and may lead to the generation of attosecond extreme ultraviolet pulses used in attosecond time-resolved spectroscopy.[1,2] More recently, such studies were extended to inorganic solids, including bulk[3,4] and low-dimensional crystals.[5,6] The related work provided insight into light field-driven electron dynamics in these systems, and their potential application as solid-state UV sources.[7–9]

Organic semiconductors (OSCs) are a group of semiconducting molecular materials, including small molecules and conjugated polymers, with quite different electronic structures from inorganic solids.[10–12] The π bonding orbitals and the antibonding π^* orbitals form the highest occupied and lowest unoccupied molecular orbitals, HOMO and LUMO, respectively, which is in analogy to the valence and

W. Li, M. Neuhaus, L. Hedewig, B. Bergues, M. F. Kling, Z. Wang
Department of Physics
Ludwig-Maximilians-Universität Munich
D-85748 Garching, Germany
E-mail: zilong.wang@lmu.de

W. Li, B. Bergues, M. F. Kling, Z. Wang
Max Planck Institute of Quantum Optics
D-85748 Garching, Germany

A. Saleh[+], M. Alharbi, H. ALQahtani, A. M. Azzeer
Physics and Astronomy Department
King Saud University
Riyadh 11451, Saudi Arabia

The ORCID identification number(s) for the author(s) of this article can be found under https://doi.org/10.1002/adom.202203070

[+]Present address: Department of Mathematics and Natural Sciences, Prince Mohammad Bin Fahd University, Al Khobar 39152, Saudi Arabia.

DOI: 10.1002/adom.202203070

M. Sharma, M. Sierka
Otto Schott Institute of Materials Research
Friedrich Schiller University Jena
D-07743 Jena, Germany

C. Hünecke, S. Gräfe
Institute of Physical Chemistry
Friedrich Schiller University Jena
D-07743 Jena, Germany

S. Gräfe
Institute of Applied Physics
and Abbe Center of Photonics, Friedrich Schiller University Jena
D-07743 Jena, Germany

S. Gräfe
Fraunhofer Institute of Applied Optics and Precision Engineering
D-07745 Jena, Germany

M. F. Kling
SLAC National Accelerator Laboratory
Menlo Park, CA 94025, USA

M. F. Kling
Applied Physics Department
Stanford University
Stanford, CA 94305, USA

A. F. Alharbi
Institute of Quantum Technologies and Advanced Computing
King Abdulaziz City for Science and Technology (KACST)
Riyadh 11442, Saudi Arabia

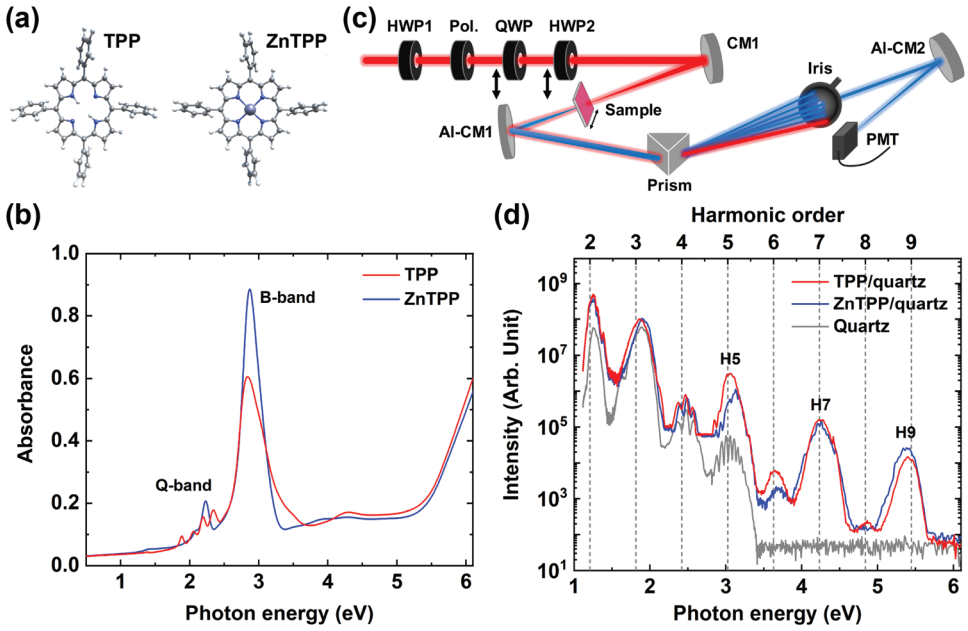

Figure 1. a) Molecular structure of TPP (left) and ZnTPP (right); b) linear absorption spectra of 100 nm thick TPP and ZnTPP films; c) experimental setup; d) high-order harmonic spectra of 100 nm thick TPP (red, solid line) and ZnTPP (blue, solid line) films as well as the bare quartz substrate (gray, solid line).

conduction band in inorganic crystals.[13] OSCs are well known to be excellent nonlinear and opto-electronic materials.[10,14] They are versatile with optical and opto-electrical properties by chemical design and synthesis,[11] and can be easily deposited to form thin films with typically tens or hundreds of nanometers thickness. These features allow for adaptable and compact on-chip devices and wide applications in integrated optics.[10] Additionally, they would serve as useful tools for harmonic generation due to the high density of emitters.[15] While significant nonlinear properties have been demonstrated in OSCs in the perturbative regime, their high-order optical response in non-perturbative regime is less studied particularly in solid-state phase. Here, we experimentally investigated below-threshold low-order harmonic emission in OSC thin films prepared from two porphyrin molecules, tetraphenylporphyrin (TPP) and one of its metallo-derivatives, ZnTPP. The insertion of different types of metal atoms into the center of the porphyrin ring could modify the electronic structures and nonlinear properties in metalloporphyrins compared to the metal-free ones.[16,17] Moreover, the TPP molecule possesses lower symmetry (D_{2h}) than the ZnTPP molecule (D_{4h}), which should enable more nonlinear wave mixing processes for the free base system than its Zn-ligated counterpart.[18,19]

Low-order harmonics in HHG can be caused by different mechanisms: 1) perturbative-type wave-mixing;[20,21] 2) intraband Bloch oscillations in the conduction band of crystalline solids;[7,22] and 3) Brunel harmonics, caused by the ionization/excitation nonlinearity with delocalized electrons moving in vicinity of atoms.[23,24] Brunel harmonics were discovered and discussed in gases,[23] and have recently attracted a renewed attention in solids.[20,24,25] More interestingly, they have been found to contain signatures of attosecond- and sub-angstrom-scale electron dynamics in the material, which can serve as a viable tool to image the reshaping of the electronic wavepacket during laser-induced tunneling.[24] In amorphous thin film OSCs, the lack of periodicity results in electronic states being localized at individual molecules.[26] Therefore, the intra-band Bloch oscillation processes can be excluded in such kind of system, facilitating the observation of Brunel harmonic generation.

Our results show that resonant and non-resonant transitions induced by near-infrared laser pulse excitation within the ZnTPP and TPP molecules yield the low-order harmonics. Experimental results are interpreted with simulations based on the real-time time-dependent density functional theory (RT-TDDFT). Herein, we utilize two slightly different implementations: the newly-developed variant based on localized Gaussian basis functions as very recently implemented in the Turbomole program package[27,28] and the commonly successfully employed variant employing real-space grids as in the Octopus program package.[29,30] We find out that an efficient transition resonant to the π–π^* excited states of the porphyrin ringsystem (accessible by a 5-photon transition) changes the nonlinear field-induced dynamics substantially, manifesting itself, for example, by a different slope in the intensity scaling. The harmonic emission from the resonant 5-photon transition, in non-perturbative light-matter interaction regime, is then attributed to the Brunel-harmonic generation.

2. Results

Tetraphenylporphyrin (TPP) and zinc tetraphenylporphyrin (ZnTPP) (from Aldrich Chem Co., purity ≥ 99%), as the investigated OSC materials, were used as received without any further purification. Molecular structures of TPP and ZnTPP can be seen in **Figure 1**a, where the (deposited) TPP molecule has D_{2h} symmetry and the ZnTPP molecule has D_{4h} symmetry with the Zn

fitted in the center of the planar tetrapyrrolic ring system.[31,32] Thin-film samples were prepared with the physical vapor deposition technique on optically flat quartz substrates in a vacuum coating system (Edwards, E306 A) under a base pressure of 10^{-6} mbar, yielding a typical film thickness of 100 nm. All the organic thin films for measurements were as-deposited samples without any further treatments. Surface topography images of both samples obtained by atomic force microscopy (AFM; see Figure S1, Supporting Information) show a homogeneous distribution of sample materials under regions of study. Both of the thin-film samples consist of randomly oriented nanorod-shape molecular packing structures dispersed in the amorphous matrix, where both parallel molecular stacking and monomer can be found in the film.[33] Linear absorption spectra of the produced TPP and ZnTPP thin films are shown in Figure 1b. Both samples exhibit the prominent B (Soret) band (2.84 eV for TPP, 2.87 eV for ZnTPP) and a weak Q-band absorption corresponding to $S_0 \rightarrow S_2$ and $S_0 \rightarrow S_1$ $\pi - \pi^*$ singlet transitions, respectively.

Below-threshold harmonic generation is measured by exciting the samples with 2 μm laser pulses from an optical parametric chirped pulse amplification (OPCPA) system, with a typical pulse duration of ≈29.7 fs (full width at half maximum, FWHM) and a repetition rate of 100 kHz (in Figure 1c).[34] A half ($\lambda/2$) waveplate (HWP1) and a wire grid polarizer were used to vary the laser intensity. An additional quarter ($\lambda/4$) waveplate (QWP) and a second half waveplate (HWP2) were added in the beam path after HWP1 and the polarizer in order to control and vary the laser ellipticity while keeping the direction of the major axis of the elliptical polarization fixed at all times. Transmitted harmonic emission was collected and focused onto a photomultiplier tube (PMT, Hamamatsu) by two UV-enhanced aluminum concave mirrors (Al-CM1 and Al-CM2). The signal of each order of harmonics was selected by a combination of a CaF_2 equilateral prism and an iris placed in front of the PMT. The measurement of harmonic emission spectra as well as the calibration of prism rotation angle were done with a UV–vis spectrometer (Ocean Optics HDX). To avoid sample degradation under high excitation intensity, a mechanical shutter was placed in front of the sample and was switched on/off between each laser excitation; the signal integration time was kept as low as possible (100 ms). Furthermore, the sample was mounted on a two-axis stage, shifting the sample position after each single measurement. The entire measurement setup was enclosed in a home-built purge box filled with nitrogen gas. In our experiment, the same measurements were repeated more than three times on different batches of samples, showing the reproducibility of the experimental results.

Measured harmonic emission spectra of TPP (red) and ZnTPP (blue) thin film samples excited at an intensity of 2.28 TW cm^{-2} are shown in Figure 1d. The fifth (H5, 3.1 eV), seventh (H7, 4.25 eV), and ninth (H9, 5.4 eV) order harmonics from both organic thin film samples can be clearly distinguished in the spectra. Emission signatures from the quartz substrate (gray) were recorded as a reference, whose contributions are seen only up to fourth order. For both samples, the H5 peaks are practically on-resonance with the B-band absorption. Weak even-harmonic emission (sixth and eighth) can be seen from samples arising from the partial breaking of inversion symmetry in the polycrystalline thin film samples with random orientation of individual molecules. The last observed harmonic, H9, lies at 5.4 eV, which is below the ionization thresholds of the two molecules that have been reported as 6.32 eV for TPP and 6.06 eV for ZnTPP.[35] We exclusively see harmonics below the ionization threshold, which ensures that the Corkum-type harmonic generation mechanism[36] for atoms and molecules, involving ionization, acceleration, and recombination, does not play a dominant role. Moreover, as we do not observe sample degradation, ionization can be considered negligible.

Molecular dynamics as well as harmonic generation processes were calculated using two different implementations of RT-TDDFT. The first set of calculations is based on our recently developed implementation of the RT-TDDFT based on localized Gaussian basis functions[27] within the Turbomole program package[28] (the Turbomole implementation hereafter). The localized basis method is able to handle large molecular systems, such as the TPP molecule, with high computing efficiency (≈10^3 CPU h $calc^{-1}$); however, ionization and field-driven continuum electronic dynamics outside the molecule cannot be addressed by employing atom-centered basis functions. It is generally well suited for the here investigated harmonic generation with energies of quanta below the ionization threshold. A low or even negligible level of ionization is confirmed with the second variant of simulation based on the well-established real-space grid-based Octopus program package (the Octopus implementation hereafter).[30] Many works have demonstrated the success of this method for the simulation of HHG in molecules or bulk solids.[6] In Octopus, electronic wavefunctions and current are calculated in real space in a spherical simulation box with a radius of 18 Å, therefore, field-driven electronic dynamics and re-combination processes following ionization are included for the proper description of HHG.

We first calculate the linear absorption spectra of single-molecule TPP and ZnTPP. As can be seen in **Figure 2**a, the calculated spectra of the individual molecules agree very well with the experimentally measured results of thin film samples, particularly in terms of the B-band absorption. Thus, in what follows, we will remain in the molecular picture (rather than evoking the bulk perspective) for the description of the harmonic generation mechanism. Harmonic emission was simulated by interaction of a 2 μm linearly polarized cosine/trapezoid-shaped laser pulse with five optical cycles (≈33 fs) and a field intensity of 1.5 TW cm^{-2}, similar to the experimental conditions, with the corresponding molecules. Laser driven electron dynamics in individual molecule were calculated starting from its electronic ground-state density at equilibrium structure optimized in vacuum. The ionization potentials and overall level of ionization of the molecules are calculated using Turbomole and Octopus, respectively. The ionization potentials of the TPP and ZnTPP molecules, calculated via Turbomole, are 6.47 and 6.51 eV, respectively, which are in reasonable agreement with the measured values.[35] And the overall ionization estimated from the loss of charges due to absorbing boundary conditions, accessed by Octopus, is very low (< 0.01%) at the experimental conditions. This is also true from experimental point of view, where sample degradation induced by the laser pulses was carefully avoided. The above two findings lend confidence to Turbomole implementation being suitable for the conditions of this study. Additionally, calculated results are almost identical with the two computational tools for most of cases (see Supporting Information for complete

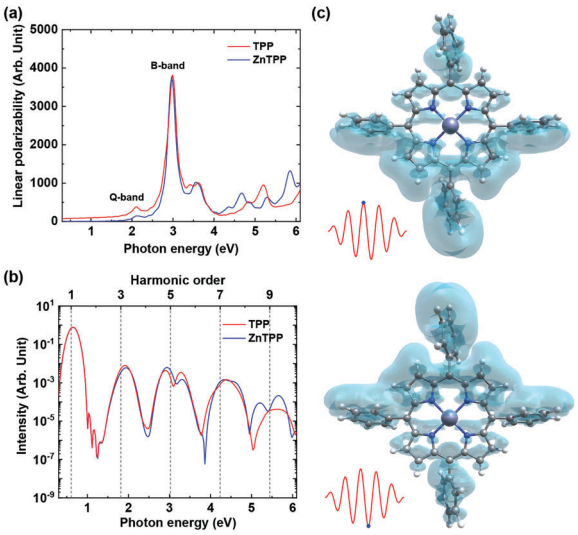

Figure 2. a) Linear absorption spectra and b) harmonic spectra of single-molecule TPP and ZnTPP obtained by Turbomole implementation; c) Isosurface snapshots of the difference between excited and ground state electronic density in ZnTPP single molecule at the maximum and minimum of the linearly polarized laser pulse (visualization via CrysX-3D Viewer[37] with isovalue $=+7 \times 10^{-5}$e Å^{-3}; also see Supporting Information for the complete animation).

numerical results). We therefore concentrate only on the results from the computationally more efficient implementation, that is, Turbomole. For those where the numerical results differ, we will evoke both results and explain the origin of the differences.

Harmonic emission spectra of TPP and ZnTPP molecules obtained from the Turbomole calculations are shown in Figure 2b. They are obtained by Fourier transforming the time-dependent dipole acceleration, $\ddot{\mu}(t)$, driven by the few-cycle laser field (see also in Figure 2c). The spectra exhibit almost identical spectral shape for both molecules except for the H5 and H9. The identical spectra, particularly in terms of the harmonic intensity from the two molecules, indicate similar electronic dynamics within the laser pulses. Indeed, the snap-shot images of electron wavepacket distributions at different times in Figure 2c reveal that the excitation is dominated by contribution from the π and π^* orbitals. The contribution of the central Zn atom's d-orbitals to the π^* orbitals of the surrounding TPP ring is minor or even negligible. Emission band splitting is observed in H5 at ≈3 eV, which can be attributed to the on-resonant $\pi \rightarrow \pi^*$ excitation at around 2.99 eV (see absorption spectra in Figure 2a). This is not seen experimentally, probably due to propagation effects, focal volume averaging, the random molecular orientation in the thin film samples, as well as resonance-enhanced multiphoton excitation and possibly ionization processes, which are not included in the modeling.

In order to obtain mechanistic insight into the origin of harmonic emission, we studied the excitation intensity dependence for each harmonic, as shown in **Figure 3**. Measured harmonic yields for H5, H7, and H9 from both TPP (red) and ZnTPP (blue) thin films are shown in Figure 3a–c. The gray scatters in the figures represent the background noise including signals contributed from emission in quartz substrate as well as stray light entering into the PMT detector. Harmonic emission from the TPP sample is significantly higher than that from the ZnTPP sample except for H9 emission. The perturbative light-matter interaction regime can be immediately identified from the $Y \propto I_{\mathrm{exc}}^{n}$ dependency in H5 and H7 (Figure 3a,b). Here I_{exc} is the excitation laser intensity and n is the harmonic order ($n = 5, 7$). For H5 and H7, the perturbative behavior dominates up to intensities of about 1.2 and 1 TW cm^{-2}, respectively. The deviation of I_{exc}^{n} at higher intensity indicates the transition from perturbative to non-perturbative interaction in the samples. For H9, only non-perturbative light-matter interaction can be seen in Figure 3c, and the almost identical harmonic signals measured in both TPP and ZnTPP samples confirm the fact that the presence of Zn cation in the porphyrin ring does not contribute significantly to the harmonic generation processes. We do not reach intensities where the signal is saturated, as this would lead to sample damage. The exceptionally larger yield for H5 from TPP compared to that from ZnTPP is attributed to ground- or excited-state reabsorption of emitted harmonic upon propagation through the thin film samples.[38] Additionally, the H5 emission exhibits an early onset of deviation of the perturbative character at comparatively low excitation intensities. This may be at first surprising and will be explained in what follows.

Simulated excitation intensity-dependent emission was obtained by integrating the spectral peaks of each order at each excitation intensity, shown in Figure 3d–f. The $Y \propto I_{\mathrm{exc}}^{n}$ dependency at relatively low excitation could be well reproduced from both RT-TDDFT implementations, further confirming that the observed harmonic emission in this regime is due to the perturbative nonlinear behavior of the molecule. Deviation from the perturbative interaction regime can be seen in H7 and H9 from both simulation methods. Interestingly, large differences between the model simulations are seen for H5: Turbomole predicts perturbative behavior for H5 throughout the intensity range while Octopus results show a saturation behavior after around 0.8 TW cm^{-2}, in a better agreement with the experimental observation. This is because the Octopus implementation calculates electron wavepackets on real-space grid basis, where ionization and the subsequent light-driven dynamics as well as recombination processes are included. In fact, a population analysis (within Octopus) shows that upon interaction with the driving field, the electronic ground state is strongly depleted. The B-band is thereby populated efficiently. However, with the resonant excitation of B-band states, transitions into multiple other electronic states, either bound or even transiently virtual states occur, thereby changing the nonlinearity substantially. This observation marks the transition from the molecular-type behavior towards the bulk-type behavior with electronic dynamics taking place in bands, formed by delocalized and degenerate electronic states of the same electronic character. A similar scenario occurs here for the large molecules, despite the obvious difference that we do not have periodic structures. We, therefore, observed the Brunel harmonic generation enhanced by resonant 5-photon transition.

An additional observation giving insight into the generation processes is the excitation ellipticity dependence of the below-threshold low-order harmonic emission. This can be seen in **Figure 4** showing the measured normalized harmonic yields of H5, H7, and H9 under different driver ellipticities in the non-perturbative regime from TPP thin film samples. Results from

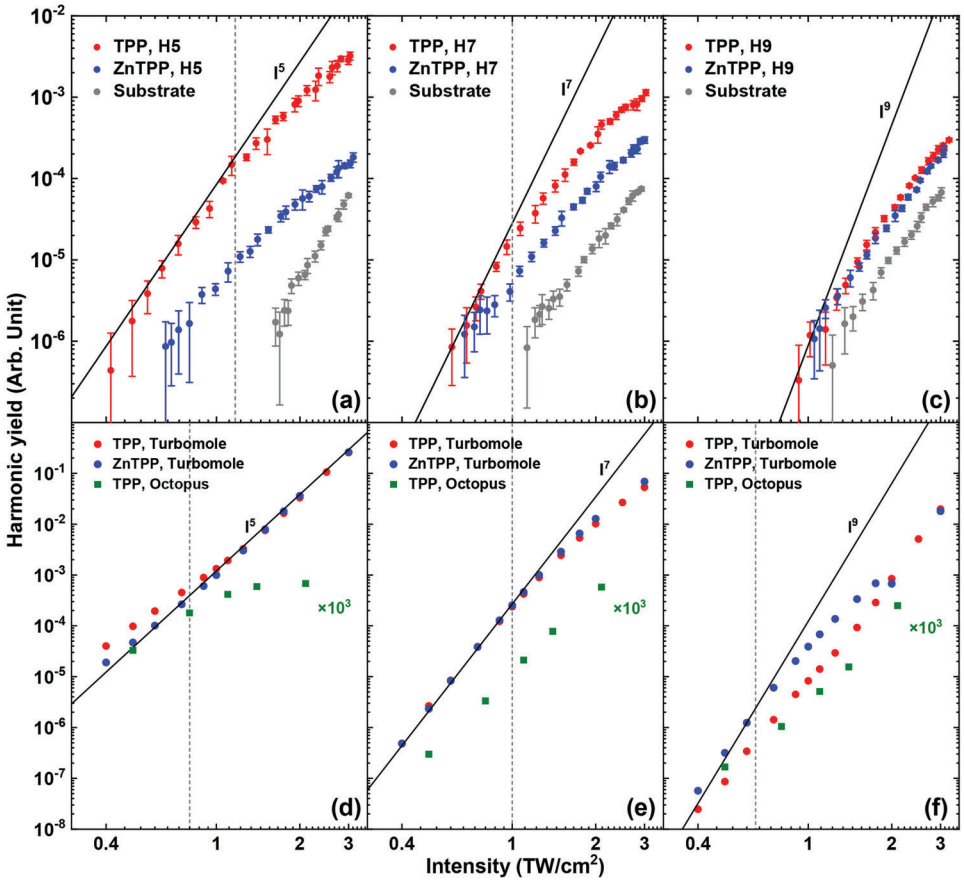

Figure 3. Excitation intensity dependence characteristics of harmonic signals in TPP and ZnTPP. Experimental results from 100 nm thin films: a) H5; b) H7; c) H9 (error bar: standard deviation of 400 measurements under the same conditions); simulation results obtained with Turbomole (red and blue dots) and Octopus (olive squares, the actual values were multiplied by 1000 for better comparison): d) H5; e) H7; f) H9.

ZnTPP samples exhibit the same trends as seen for TPP, and are therefore only shown in the Supporting Information. In the experiment, the driver ellipticity, ϵ_d, of exciting laser pulses is varied from 0 (linearly polarized) to 1 (circularly polarized) while keeping the total intensity and major axis fixed. For all harmonics, the maximum yield occurs for linearly polarized excitation while nearly no signal can be measured for circularly polarized excitation. The harmonic yield decreases faster with ellipticity for increasing harmonic orders. The ellipticity-dependent harmonic emission behavior can be well fitted by the Gaussian function $e^{-\epsilon_d^2/\sigma_n^2}$, where ϵ_d is the driver ellipticity and σ_n (n= 5,7,9) is fitting parameter.[39] A lower σ_n represents higher sensitivity of the harmonic yield to the excitation ellipticity. This behavior can be explained by the increase of the non-perturbative character from H5 to H9. Moreover, the much narrower width of H9, which lies energetically only a little below the ionization threshold, points toward a higher contribution of (transient) ionization to the signal. The relatively shallow ellipticity dependence of H5 can be explained by the role of the resonance, in terms of the Brunel harmonic generation in non-perturbative regime: as the transition of the $\pi \rightarrow \pi^*$ state is dipole-allowed within the plane, for almost all ellipiticities, the electronic state can be coherently excited, thereby driving a wavepacket. Additionally, the measured ellipticity dependence still features a narrower peak than that of the simulated results by Turbomole on H7, shown in Figure 4, suggesting that atomic-like transient ionization processes should be involved in the harmonic generation processes for other harmonic orders.[40–42]

3. Conclusion

We have demonstrated Brunel harmonic generation in TPP and ZnTPP thin films in the strong-field driven non-perturbative regime. With the help of RT-TDDFT based calculations using the Turbomole and Octopus program packages, we identify the origin of unusual scaling of the fifth harmonic to be caused by excitation to a bright, resonant electronic state (the B-band) of the molecule, which changes the underlying dynamics substantially: the 5-photon resonant state causes a strong depletion of the electronic ground state of the molecule with significant population of this excited state and large contribution of many other bound (and quasi-free transient) excited electronic states. This results in a strong deviation from the perturbative mechanism of harmonic generation, seen in not only the intensity scaling but also the ellipticity dependence. The B-band is energetically so broad that excitation into it leads to dynamics resembling bulk-like behavior. In addition, upon light propagation through the sample,

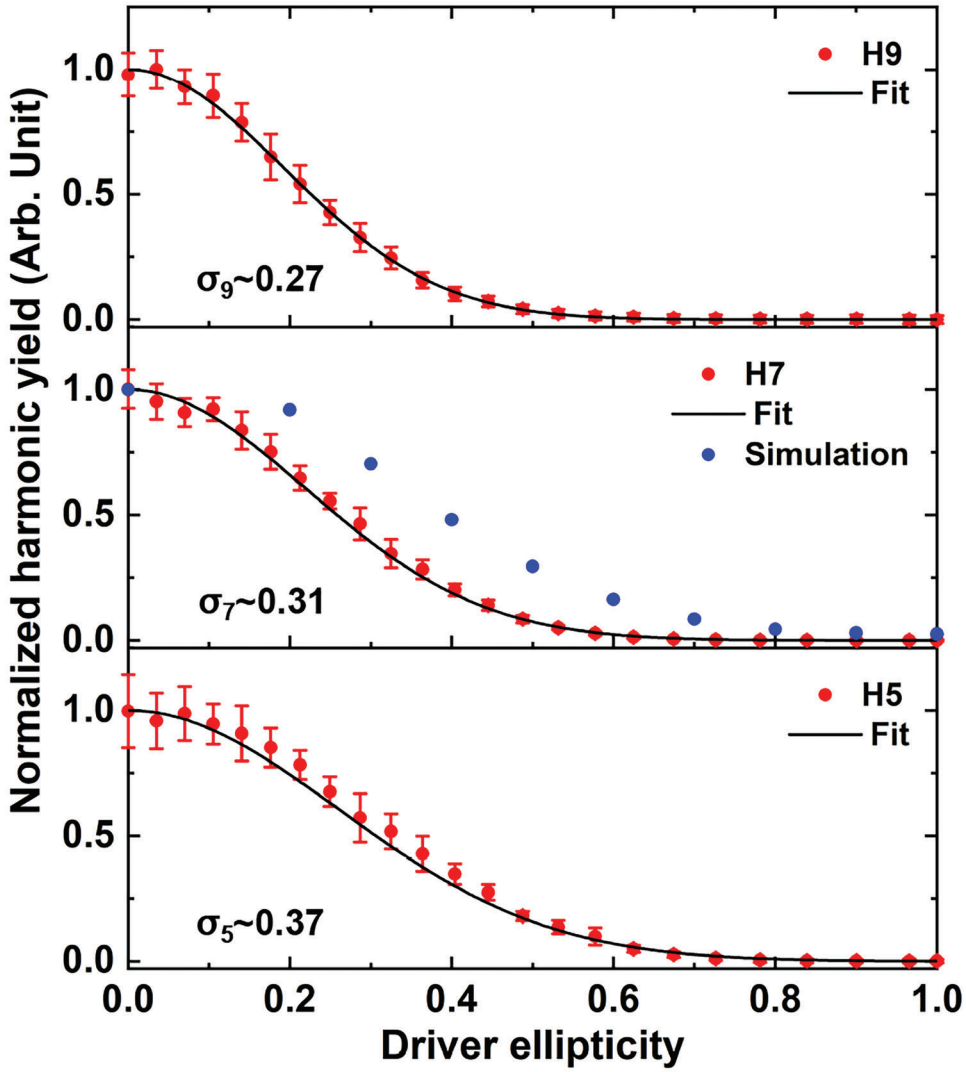

Figure 4. Excitation ellipticity dependence characteristics of high harmonic signals in 100-nm thick TPP: normalized high harmonic yields (red dots) versus driver ellipticity, a Gaussian function fitting (black solid line), and simulation results obtained from Turbomole implementation (blue dots).

it can be efficiently re-absorbed and re-emitted, changing the observed features even further. In contrast, the ninth harmonic lies energetically closely around the ionization threshold, therefore, partial (transient) ionization cannot be neglected anymore in order to fully describe its mechanistic details. Our findings show the potential of OSCs, TPP and ZnTPP in our case, as high frequency up-conversion emitters. Such emitters would be applicable in integrated photonic and opto-electronic devices with the help of mature device fabrication techniques.

4. Experimental Section

RT-TDDFT Calculation Method: Electron density $\rho(\mathbf{r}, t)$ at time t was obtained in RT-TDDFT by solving the single-particle time-dependent Kohn Sham (KS) equations

$$i\frac{\partial \psi_m(\mathbf{r}, t)}{\partial t} = \left[-\frac{\nabla^2}{2} + \nu_{\text{eff}}^{\text{KS}}(\mathbf{r}, t)\right]\psi_m(\mathbf{r}, t) \quad (1)$$

where $\psi_m(\mathbf{r}, t)$ are the time-dependent KS molecular orbitals (MO) and $\nu_{\text{eff}}^{\text{KS}}[\rho](\mathbf{r}, t)$ is the time-dependent effective KS potential that consists of nuclear-electron ν_{ne}, exchange-correlation $\nu_{\text{xc}}[\rho]$ (with adiabatic approximation), electron-electron $\nu_{\text{J}}[\rho]$ and external field $\nu_{\text{E}}(t)$ potentials. In practical implementations, the time dependent KS equations were reformulated in terms of the Liouville-von Neumann (LvN) equation

$$i\frac{\partial \mathbf{D}(t)}{\partial t} = [\mathbf{F}(t), \mathbf{D}(t)] \quad (2)$$

where $\mathbf{F}(t)$ and $\mathbf{D}(t)$ are the time-dependent KS potential in matrix form and the single electron reduced density matrix, respectively in the orthonormal basis of MO. The density matrix $\mathbf{D}(t)$ could be propagated in time by numerically integrating the LvN equation using a variety of methods.[43]

The Turbomole implementation employed the Magnus expansion, which is a popular method in terms of performance and stability, especially for implementations based on localized basis functions. The readers are referred to previous work by the authors,[27] for further details. It should be noted that the implementation lacks a way to treat the

ionization losses or the spurious reflections of the electronic wavefunction due to the incompleteness of the basis set. Usually, either a real space complex absorbing potential (CAP)[44–47] or heuristic lifetime model[47] applied to electronic-state energies was employed to tackle the aforementioned issue. Furthermore, for a better representation of continuum states extending over large distances, the Gaussian basis sets were usually augmented with basis functions centered on ghost atoms far from the molecule[47–49] or a large number of diffuse basis functions. A lot of research had gone into improving Gaussian functions based basis sets for a better description of the continuum states.[48,50–52] While beneficial, the aforementioned strategies were mainly relevant for the study of HHG beyond I_p, which is not the case in this study.

The Octopus programming package was also utilized to simulate the harmonic response of the molecules. The major difference between the two is the fact that Turbomole employs a representation of the KS-wavefunctions by a basis-set of Gaussian functions while Octopus' wavefunctions are defined on the real space grid. This approach had the advantage that continuum dynamics like ionization and recombination, inherently part of HHG of finite systems, could be readily included by choosing a larger simulation box though this comes at the cost of a greater computational effort due to larger grid sizes. The computational details of both implmentations are included in the Supporting Information.

HHG Spectra Calculation: The HHG spectrum from local-basis RT-TDDFT simulations was calculated by Fourier transforming the time-dependent dipole acceleration $\ddot{\mu}(t)$ (second derivative of the expectation value of induced dipole moment with regard to time)[53,54]

$$P(\omega) = \left| \frac{1}{t_f - t_i} \int_{t_i}^{t_f} \frac{\mathrm{d}^2 \mu^{\mathrm{ind}}(t)}{\mathrm{d}t^2} \mathrm{e}^{-i\omega t} \, \mathrm{d}t \right|^2 \tag{3}$$

The time-dependent induced dipole moment is given as

$$\mu_j^{\mathrm{ind}}(t) = \mu_j(t) - \mu_j^0 \quad , \quad j = x, y, z \tag{4}$$

where μ_0^j is the dipole moment of the unperturbed system and

$$\mu_j(t) = \mathrm{Tr}\left[\mathbf{M}^j \cdot \mathbf{D}(t)\right], \quad j = x, y, z \tag{5}$$

with $\mathbf{M}^j$ and $\mathbf{D}$ being the dipole moment and density matrices, respectively.

The harmonic spectra P_j of Octopus were obtained from the total charge current $\mathbf{J}(\mathbf{r}, t)$ following the equation:

$$P_j(\omega) = \omega^2 \left| \int \mathbf{J}(\mathbf{r}, t) \mathrm{e}^{-i\omega t} \right|^2 \tag{6}$$

Supporting Information

Supporting Information is available from the Wiley Online Library or from the author.

Acknowledgements

W.L. and A.S. contributed equally to this work. The authors are grateful for support by King-Saud University within the MPQ-KSU collaboration. W.L. acknowledges support by the Max Planck Society via the IMPRS for Advanced Photon Science. M.F.K. acknowledges support by the Max Planck Society via the Max Planck Fellow program. M.F.K.'s work at SLAC is supported by the U.S. Department of Energy, Office of Science, Basic Energy Sciences, Scientific User Facilities Division, under Contract No. DE-AC02-76SF00515. M.A., A.M.A., A.F.A. acknowledge the Researchers Supporting Project (RSP2023R152), King Saud University, Riyadh, Saudi Arabia. Z.W. is grateful for support by a startup grant from the SPP QUTIF funded by the German Research Foundation and for support by the Alexander von Humboldt Foundation. M.Sh. and M.Si. gratefully acknowledge financial support from the Turbomole GmbH as well as the German Research foundation DFG (CRC 1375 NOA, project number 398816777) project A4. M.Sh., C.H., M.N., S.G., and M.F.K. are grateful for support by the German Research Foundation DFG (CRC 1375 NOA, project number 398816777) projects A1, A4 and B1. S.G. highly ackowledges funding by the European Research Council via the ERC Consolidator Grant "Quem-Chem," grant number 772776.

Open access funding enabled and organized by Projekt DEAL.

Conflict of Interest

The authors declare no conflict of interest.

Data Availability Statement

The data that support the findings of this study are available in the supplementary material of this article.

Keywords

high harmonic generation, organic semiconductors, resonance effect, strong light–matter interaction

Received: December 21, 2022
Revised: April 14, 2023
Published online: May 21, 2023

[1] F. Krausz, M. Ivanov, *Rev. Mod. Phys.* **2009**, *81*, 163.
[2] J. Li, J. Lu, A. Chew, S. Han, J. Li, Y. Wu, H. Wang, S. Ghimire, Z. Chang, *Nat. Commun.* **2020**, *11*, 2748.
[3] S. Ghimire, A. D. DiChiara, E. Sistrunk, P. Agostini, L. F. DiMauro, D. A. Reis, *Nat. Phys.* **2011**, *7*, 138.
[4] Y. S. You, D. A. Reis, S. Ghimire, *Nat. Phys.* **2017**, *13*, 345.
[5] N. Yoshikawa, T. Tamaya, K. Tanaka, *Science* **2017**, *356*, 736.
[6] N. Tancogne-Dejean, A. Rubio, *Sci. Adv.* **2018**, *4*, eaao5207.
[7] E. Goulielmakis, T. Brabec, *Nat. Photonics* **2022**, *16*, 411.
[8] S. Ghimire, D. A. Reis, *Nat. Phys.* **2019**, *15*, 10.
[9] Y. S. You, Y. Yin, Y. Wu, A. Chew, X. Ren, F. Zhuang, S. Gholam-Mirzaei, M. Chini, Z. Chang, S. Ghimire, *Nat. Commun.* **2017**, *8*, 724.
[10] S. Ahmad, *J. Polym. Eng.* **2014**, *34*, 279.
[11] H. Bronstein, C. B. Nielsen, B. C. Schroeder, I. McCulloch, *Nat. Rev. Chem.* **2020**, *4*, 66.
[12] T. Okamoto, S. Kumagai, E. Fukuzaki, H. Ishii, G. Watanabe, N. Niitsu, T. Annaka, M. Yamagishi, Y. Tani, H. Sugiura, T. Watanabe, S. Watanabe, J. Takeya, *Sci. Adv.* **2020**, *6*, eaaz0632.
[13] G. Horowitz, *J. Appl. Phys.* **2015**, *118*, 115502.
[14] M. O. Senge, M. Fazekas, E. G. Notaras, W. J. Blau, M. Zawadzka, O. B. Locos, E. M. Ni Mhuircheartaigh, *Adv. Mater.* **2007**, *19*, 2737.
[15] A. Saleh, W. Li, H. ALQahtani, M. Neuhaus, A. Alshehri, B. Bergues, M. Alharbi, M. F. Kling, A. M. Azzeer, Z. Wang, A. F. Alharbi, *Results Phys.* **2022**, *37*, 105513.
[16] W. Blau, H. Byrne, W. Dennis, J. Kelly, *Opt. Commun.* **1985**, *56*, 25.
[17] K. McEwan, K. Lewis, G.-Y. Yang, L.-L. Chng, Y.-W. Lee, W.-P. Lau, K.-S. Lai, *Adv. Funct. Mater.* **2003**, *13*, 863.
[18] G. N. Ngubeni, J. Britton, J. Mack, E. New, I. Hancox, M. Walker, T. Nyokong, T. S. Jones, S. Khene, *J. Mater. Chem. C* **2015**, *3*, 10705.
[19] C. Bao, Y. Li, Y. Li, Z. Si, Y. Zhang, C. Chen, L. Wang, Q. Duan, *New J. Chem.* **2021**, *45*, 16030.
[20] P. Jürgens, B. Liewehr, B. Kruse, C. Peltz, D. Engel, A. Husakou, T. Witting, M. Ivanov, M. Vrakking, T. Fennel, A. Mermillod-Blondin, *Nat. Phys.* **2020**, *16*, 1035.

[21] W.-H. Xiong, L.-Y. Peng, Q. Gong, *J. Phys. B: At. Mol. Opt. Phys.* **2017**, *50*, 032001.
[22] G. Vampa, T. Brabec, *J. Phys. B: At. Mol. Opt. Phys.* **2017**, *50*, 083001.
[23] F. Brunel, *J. Opt. Soc. Am. B* **1990**, *7*, 521.
[24] I. Babushkin, Á. J. Galán, J. R. C. de Andrade, A. Husakou, F. Morales, M. Kretschmar, T. Nagy, V. Vaičaitis, L. Shi, D. Zuber, L. Bergé, S. Skupin, I. A. Nikolaeva, N. A. Panov, D. E. Shipilo, O. G. Kosareva, A. N. Pfeiffer, A. Demircan, M. J. J. Vrakking, U. Morgner, M. Ivanov, *Nat. Phys.* **2022**, *18*, 417.
[25] P. Jürgens, B. Liewehr, B. Kruse, C. Peltz, T. Witting, A. Husakou, A. Rouzee, M. Ivanov, T. Fennel, M. J. Vrakking, A. Mermillod-Blondin, *ACS Photonics* **2022**, *9*, 233.
[26] S. D. Baranovskii, *Phys. Status Solidi B* **2014**, *251*, 487.
[27] C. Müller, M. Sharma, M. Sierka, *J. Comput. Chem.* **2020**, *41*, 2573.
[28] S. G. Balasubramani, G. P. Chen, S. Coriani, M. Diedenhofen, M. S. Frank, Y. J. Franzke, F. Furche, R. Grotjahn, M. E. Harding, C. Hättig, A. Hellweg, B. Helmich-Paris, C. Holzer, U. Huniar, M. Kaupp, A. M. Khah, S. K. Khani, T. Müller, F. Mack, B. D. Nguyen, S. M. Parker, E. Perlt, D. Rappoport, K. Reiter, S. Roy, M. Rückert, G. Schmitz, M. Sierka, E. Tapavicza, D. P. Tew, et al., *J. Chem. Phys.* **2020**, *152*, 184107.
[29] A. Castro, A. Rubio, E. K. U. Gross, *Eur. Phys. J. B* **2015**, *88*, 191.
[30] X. Andrade, D. Strubbe, U. De Giovannini, A. H. Larsen, M. J. Oliveira, J. Alberdi-Rodriguez, A. Varas, I. Theophilou, N. Helbig, M. J. Verstraete, L. Stella, F. Nogueira, A. Aspuru-Guzik, A. Castro, M. A. L. Marques, A. Rubio, *Phys. Chem. Chem. Phys.* **2015**, *17*, 31371.
[31] M. Gouterman, *J. Mol. Spectrosc.* **1961**, *6*, 138.
[32] D. Marsh, L. Mink, *J. Chem. Educ.* **1996**, *73*, 1188.
[33] X.-L. Zhang, J.-W. Jiang, Y.-T. Liu, S.-T. Lou, C.-L. Gao, Q.-Y. Jin, *Sci. Rep.* **2016**, *6*, 22756.
[34] M. Neuhaus, H. Fuest, M. Seeger, J. Schötz, M. Trubetskov, P. Russbueldt, H. Hoffmann, E. Riedle, Z. Major, V. Pervak, M. F. Kling, P. Wnuk, *Opt. Express* **2018**, *26*, 16074.
[35] Y. Nakato, K. Abe, H. Tsubomura, *Chem. Phys. Lett.* **1976**, *39*, 358.
[36] P. B. Corkum, *Phys. Rev. Lett.* **1993**, *71*, 1994.
[37] M. Sharma, D. Mishra, *J. Appl. Crystallogr.* **2019**, *52*, 1449.
[38] L. Jiang, T. Jiu, Y. Li, Y. Li, J. Yang, J. Li, C. Li, H. Liu, Y. Song, *J. Phys. Chem. B* **2008**, *112*, 756.
[39] C. Liu, Y. Zheng, Z. Zeng, R. Li, *Phys. Rev. A* **2016**, *93*, 043806.
[40] B. Shan, S. Ghimire, Z. Chang, *Phys. Rev. A* **2004**, *69*, 021404.
[41] T. Kanai, S. Minemoto, H. Sakai, *Phys. Rev. Lett.* **2007**, *98*, 053002.
[42] A. F. Alharbi, A. E. Boguslavskiy, N. Thiré, G. S. Thekkadath, S. Patchkovskii, B. E. Schmidt, F. Légaré, T. Brabec, V. R. Bhardwaj, M. Spanner, *Phys. Rev. A* **2017**, *96*, 043402.
[43] A. Castro, M. A. Marques, A. Rubio, *J. Chem. Phys.* **2004**, *121*, 3425.
[44] R. Kosloff, D. Kosloff, *J. Comput. Phys.* **1986**, *63*, 363.
[45] U. V. Riss, H. Meyer, *J. Chem. Phys.* **1996**, *105*, 1409.
[46] D. E. Manolopoulos, *J. Chem. Phys.* **2002**, *117*, 9552.
[47] F. Bedurke, T. Klamroth, P. Saalfrank, *Phys. Chem. Chem. Phys.* **2021**, *23*, 13544.
[48] E. Coccia, B. Mussard, M. Labeye, J. Caillat, R. Taïeb, J. Toulouse, E. Luppi, *Int. J. Quantum Chem.* **2016**, *116*, 1120.
[49] E. Coccia, R. Assaraf, E. Luppi, J. Toulouse, *J. Chem. Phys.* **2017**, *147*, 014106.
[50] E. Coccia, E. Luppi, *Theor. Chem. Acc.* **2016**, *135*, 43.
[51] A. P. Woźniak, M. Lesiuk, M. Przybytek, D. K. Efimov, J. S. Prauzner-Bechcicki, M. Mandrysz, M. Ciappina, E. Pisanty, J. Zakrzewski, M. Lewenstein, R. Moszyński, *J. Chem. Phys.* **2021**, *154*, 094111.
[52] C. Witzorky, G. Paramonov, F. Bouakline, R. Jaquet, P. Saalfrank, T. Klamroth, *J. Chem. Theory Comput.* **2021**, *17*, 7353.
[53] M. Labeye, F. Zapata, E. Coccia, V. Véniard, J. Toulouse, J. Caillat, R. Taïeb, E. Luppi, *J. Chem. Theory Comput.* **2018**, *14*, 5846.
[54] F. Bedurke, T. Klamroth, P. Krause, P. Saalfrank, *J. Chem. Phys.* **2019**, *150*, 234114.